UC Berkeley
UC Berkeley Previously Published Works

Title
Lithium nitrate: A double-edged sword in the rechargeable lithium-sulfur cell

Permalink
https://escholarship.org/uc/item/4r94t7wh

Authors
Ye, Yifan
Song, Min-Kyu
Xu, Yan
et al.

Publication Date
2019

DOI
10.1016/j.ensm.2018.09.022

Peer reviewed

eScholarship.org Powered by the California Digital Library
University of California

Lithium Nitrate: A Double-edged Sword in the Rechargeable Lithium-Sulfur Cell

Abstract: Lithium nitrate ($LiNO_3$) has been the most studied electrolyte additive in lithium-sulfur (Li-S) cells, due to its known function of suppressing the shuttle effect in Li-S cells, which provides a significant increase in the cell's coulombic efficiency and cycling stability. Previous studies indicated that $LiNO_3$ participated in the formation of a passive layer on the lithium electrode and thus suppressed the redox shuttle of the dissolved polysulfides. However, the effects of the $LiNO_3$ on the positive electrode materials have rarely been investigated. By combining scanning electron microscopy (SEM), element-selective X-ray absorption spectroscopy, and electrochemical characterizations, we performed a comprehensive study of how the $LiNO_3$ altered the properties of the sulfur electrode/electrolyte interface in Li-S cells and thus influenced the cell performance. We found that $LiNO_3$ is a double-edged sword in the Li-S cell: on one hand, it increased the consumption of the active sulfur; on the other hand, it promoted the survival of the carbon matrix constituent in the sulfur electrode. These two competitive effects indicated that a proper moderate concentration of $LiNO_3$ is required to achieve an optimized cell performance.

Key Words: Lithium-Sulfur cell; lithium nitrate; cathode-electrolyte interface; X-ray absorption spectroscopy; double-edged sword effect

1. Introduction:

Increasing interest in the electric transportation sector and bulk energy storage systems have fueled a growth in the demand for high–performance rechargeable energy storage devices with high capacity and high specific

energy. The lithium-sulfur (Li-S) cell is a promising prospect for electrochemical energy storage owing to its high theoretical specific capacity (1675 mAh/g), which is about 10 times higher than that of commercial Li ion cells using lithiated transition metal oxides and phosphates as cathode materials. However, there are technical challenges that preclude the widespread applications of the Li-S cells.[1-4] One of the main obstacles is that the Li-S cell suffers from a polysulfide shuttle effect that limits the practical capacity of the sulfur cathodes and causes rapid capacity decay.[5-8] The notorious shuttle effect originates from the high solubility of lithium polysulfides (PS), a series of sulfur electrode intermediates, in organic solvents, and from the high reactivity between the dissolved PS and Li anode. The dissolution of PS in organic electrolytes is inevitable because chemical reactions of the sulfur electrode mainly take place at the solid-liquid (electrode-electrolyte) interface between the electrolyte with dissolved PS and solid cathode materials. To take full advantage of the Li-S cell, the polysulfide shuttle effect should be suppressed. A breakthrough in the protection of the Li-S cell from shuttle effect is the discovery of $LiNO_3$ as an additive in liquid electrolytes.[9-11] The $LiNO_3$ salt has been regarded as the most effective shuttle suppressor.

The function of $LiNO_3$, according to the prevailing understanding, is to form a solid electrolyte interface (SEI) layer on the surface of the Li electrode via a spontaneous reaction.[12-20] This protective layer, identified as Li_xNO_y, efficiently minimizes PS shuttle effect by protecting the lithium anode from chemical reaction with the dissolved PS and preventing the PS from electrochemical reduction on the Li surface. Additionally, $LiNO_3$ can also act as a stabilizing additive in the Li-S cell by reducing the generation of CH_4 and/or H_2, which are the major gaseous decomposition products[21]. More recently, several groups have argued that the function of the $LiNO_3$ on the sulfur electrode should also be considered.

Xu et al. found that a Li-S cell containing a pre-$LiNO_3$-treated Li anode and a sulfur cathode cycling in $LiNO_3$-free electrolyte did not suppress the shuttle

effect efficiently, indicating that the robust Li passivation layer is not the only factor causing the enhanced cell performance.[22] Moreover, Zhang et al. argued that $LiNO_3$ plays multi-roles at the sulfur electrode: $LiNO_3$ can adversely affect the cell performance by forming reduction products at potentials lower than 1.6 V; on the other hand $LiNO_3$ can catalyze the conversion of long-chain PS to elemental S, which is beneficial to the cell performance.[16, 18, 19, 23]

Based on these observations, it is well accepted that adding $LiNO_3$ to the electrolyte can indeed significantly affect the electrode-electrolyte interfacial properties. While the anode-electrolyte SEI layer has been widely investigated,[24-26] the cathode/electrolyte interface (CEI) has not been directly investigated to obtain detailed knowledge on how the $LiNO_3$ affects the cathode material.

In this work, we probe directly the CEI layer using X-ray absorption spectroscopy (XAS). Benefiting from the element-resolved and chemical environmental-sensitive properties of XAS, various sulfur electrode constituents can be investigated individually.[27-31] Combining the spectroscopic investigations and electrochemical characterizations on Li-S cells with electrolyte containing various concentrations of $LiNO_3$ during long-term cycling we are able to provide new insights on how the $LiNO_3$ in the electrolyte can alter the properties of the CEI layer and thus influence the cell performance.

2. Material and methods:

2.1 Cell assembly and testing

The cell assembly and electrochemical characterization process were recorded in the supporting information. Basically, the Li-S cells were constructed by combining the CTAB-modified S−GO nanocomposite with an elastomeric styrene butadiene rubber /carboxy methyl cellulose (SBR/CMC) binder as positive electrode, lithium metal foil (99.98%, Cyprus Foote Mineral) as negative electrode, and an ionic liquid based novel electrolyte

containing $LiNO_3$ additive as electrolyte. The synthesis of the CTAB-modified S-GO nano-compositions has been reported in our previous work.[1, 28] Electrolytes containing 0.1 M, 0.5 M, and 1.0 M $LiNO_3$ have been investigated in each set of experiments. Galvanostatic discharge and charge cycling between 1.5 V and 2.8 V was performed using a battery cycler (Maccor Series 4000). The cells were cycled at a discharge rate of 1 C (1C= 1675 mA/g S), while the charge rates of 0.5 C and 1.0 C have been applied to charge two sets of cells. Additionally, to check the specific capacity that can be obtained at a lower C-rate, cells were checked periodically during the long-term cycling test, the specific capacity of the cells was measured at the 500^{th}, 800^{th}, and 1000^{th} cycle with a charge/discharge rate of 0.05 C/0.05 C. The cells charged at 0.5 C were denoted as C-0.1, C-0.5 and C-1.0, respectively, based on the concentrations of $LiNO_3$ used in the electrolyte; while the cells charged at 1.0 C were denoted as CH-0.1, CH-0.5, and CH-1.0. The cell capacity was normalized by the weight of sulfur, determined by measuring the TGA weight loss to 600 ^{o}C. Before all electrochemical characterizations, the cells were held at open circuit at room temperature for 24 hrs. All electrochemical characterizations were performed inside a test chamber (TestEquity TEC1) maintained at 30 ^{o}C. After several charge/discharge cycles, the cells were stopped at the fully charged state at 2.8 V. After that, the cell was disassembled, and the sulfur electrodes were washed with DOL-DME three times to clean up the surface.

2.2 Imaging test

SEM images were taken with a Zeiss Gemini Ultra-55 instrument with an accelerating voltage of 10 kV using the high vacuum mode at room temperature.

2.3 Surface- and bulk- sensitive X-ray absorption spectra

The cleaned sulfur electrodes were transferred to the vacuum chamber for the XAS measurements. S K-edge XAS spectra were measured at three beamlines, namely, BL5.3.1, BL9.3.1, and BL10.3.2 at the Advanced Light Source, Lawrence Berkeley National Laboratory. C K-edge XAS spectra were

measured at the BL8.0.1. The total electron yield (TEY) and total fluorescence yield (TFY) signals were recorded simultaneously during the XAS measurements, providing surface and bulk sensitive characterizations, respectively. TEY signals were recorded by monitoring the sample drain current, whereas TFY signals were collected using a channeltron detector at C K-edge and silicon drift detector at S K-edge, respectively. The energy scale for the S K-edge was calibrated using elemental S spectra assuming the white line to be at 2472.2 eV, whereas the energy scale for the C K-edge was calibrated to the graphene oxide spectra assuming the π* peak to be at 285.5 eV.

Both TEY and TFY XAS spectra were normalized to the incoming photon flux, represented by the drain current measured from an upstream gold mesh and ionic chamber for C K-edge and S K-edge, respectively. A linear background based on the slope in the pre-edge region was subtracted from each flux-normalized XAS spectrum, which was then normalized again to the post-edge region. Quantitative deconvolution of spectra was performed by using software Athena Demeter version 0.9.24.

3. Results and Discussion:

Figure 1 (a) and (b) display the discharge capacity and coulombic efficiency of the S electrode with different electrolytes. The capacities reached the highest values after tens of charge-discharge cycles and delivered initial capacities of 724 mA·h/g, 734 mA·h/g, and 794 mA·h/g at charge/discharge rates of 0.5C/1.0C for cells C-0.1, C-0.5, and C-1.0. The capacities dropped to 293 mA·h/g, 436 mA·h/g, and 262 mA·h/g, respectively, after 1000 cycles. Figure 1 (b) shows the coulombic efficiency of the Li-S cells containing different concentrations of $LiNO_3$. For cell C-0.1, the coulombic efficiency dropped from 100% to 98.2% in the first 50 cycles and then gradually decreased to 96.5% at the 1000^{th} cycle; for the cell C-0.5, nearly 100% coulombic efficiency was obtained; finally, for the cell C-1.0, the coulombic efficiency is 100% in the first 800 cycles and then slightly decreased to 99.5% in the last 200 cycles.

Figure 1 (c)-(e) show the representative discharge voltage profiles of Li-S cells using the electrolytes containing 0.1 M. 0.5 M, and 1.0 M $LiNO_3$ in the voltage window of 1.5-2.8 V at the charge/discharge rate of 0.05C/0.05C at the 500^{th}, 800^{th}, and 1000^{th} cycle, respectively. The voltage-capacity curve of all the three cells exhibited two discharge plateaus at around 2.3 V and 2.1 V, corresponding to the formation of long chain and short chain polysulfides, respectively.[1, 5] These results represent a highly reversible sulfur electrochemical reaction during the cell charge-discharge process, and indicate that similar reactions occurred during the cell cycling process regardless of the $LiNO_3$ concentration. The specific capacity values of the cells at different cycles recorded in Figure 1 (f) indicated that the cell C-0.5 delivered the highest specific discharge capacity at the 500^{th}, 800^{th}, and 1000^{th} cycle compared to those of cells C-0.1 and C-0.5. The difference of the delivered specific capacity between the cell C-0.1 and cell C-1.0 is not significant in the 500^{th} cycle; with further cycling, the cell C-0.1 delivered higher specific energy compared to that of the cell C-1.0 in the 800^{th} cycle; this difference became more obvious at the 1000^{th} cycle. Furthermore, by normalizing the specific capacity values to the value at the 500^{th} cycle (Figure 1 (g)), the decay rates of the specific capacity of cell C-0.5 and C-1.0 were the slowest and fastest, respectively.

In summary, it can be concluded that: (1) a high concentration of $LiNO_3$ in the electrolyte helps to retain high coulombic efficiency (~100%); (2) cells with electrolyte containing a moderate concentration of $LiNO_3$ delivered better cell capacity and cycling stability, while adding either too high (1.0 M) or too low (0.1 M) amounts of $LiNO_3$ in the electrolyte did not show any advantages.

According to conventional understanding, $LiNO_3$ can extensively react with the lithium electrode and reduce its reaction with the polysulfides to inhibit the shuttle effect. This procedure led to the continuous consumption of the $LiNO_3$ during the cell cycling process, which suggested that the electrolyte containing high concentration of $LiNO_3$ is favored to get good performance, especially when targeting for a long-term cycle life.[17, 19, 22] This proposed scheme is contrary to the result that the cell performance exhibited a volcano-shaped dependence on the $LiNO_3$ concentration. Thus, new insights of how $LiNO_3$ influenced the CEI layer structures and cell performances are needed. As a complement to the current researches, mostly focusing on the influence of $LiNO_3$ on the SEI layer, we want to focus on the changes of the interfacial layer between the sulfur electrode and electrolyte as a function of $LiNO_3$ concentration in this work.

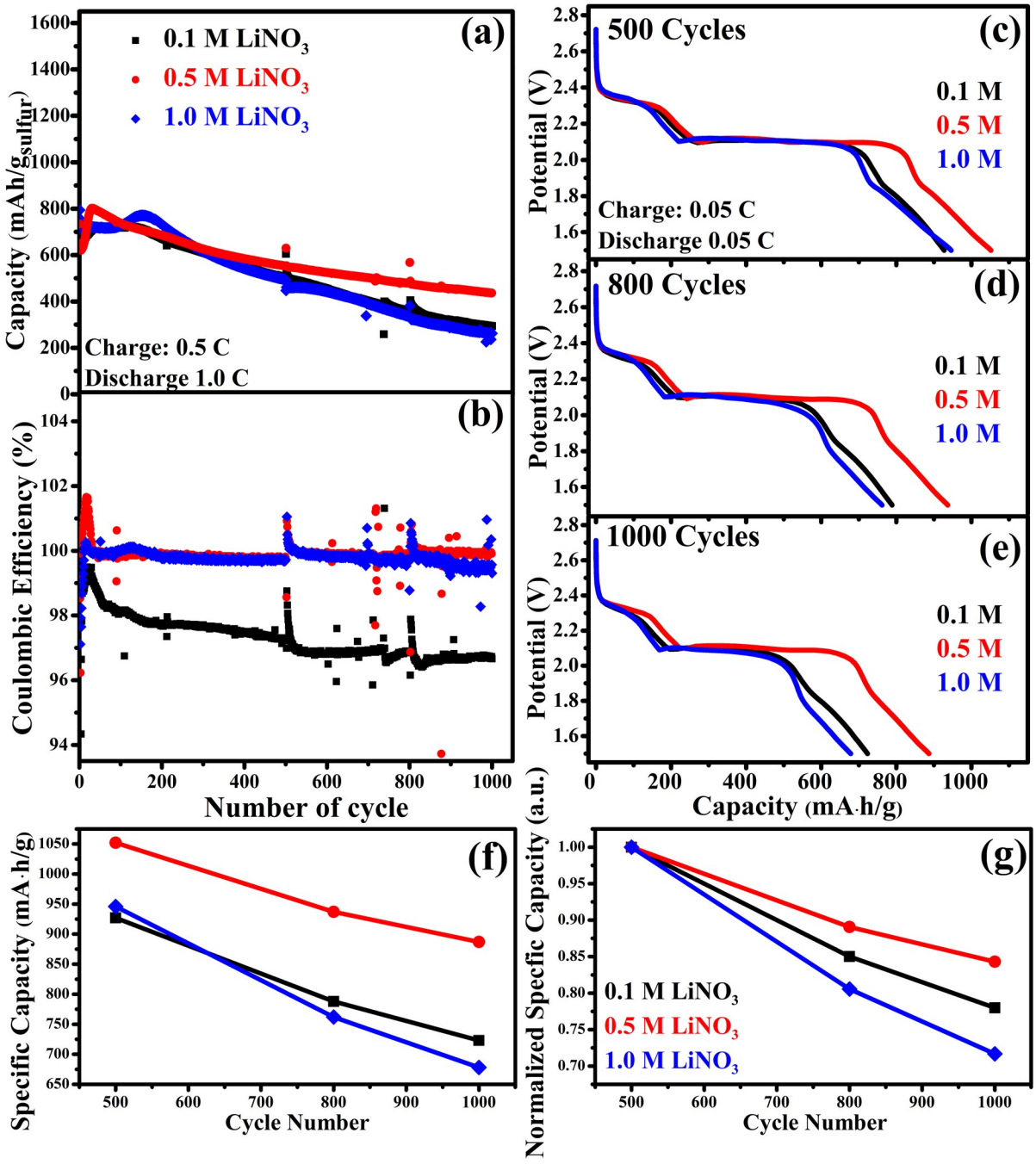

192

193 **Figure 1: The electrochemical characterization of the Li-S cells with different**
194 **concentrations of $LiNO_3$ in the electrolyte. (a) Cycling performance and (b)**
195 **Coulombic efficiency of Li-S cells with 0.1 M, 0.5 M, and 1.0 M $LiNO_3$ containing**
196 **electrolyte at charge/discharge rate of 0.5 C/1.0 C. (c)-(e) Discharge voltage**
197 **profiles at different cycles of the three cycles at 0.05 C. (f) The specific capacity**
198 **and (g) normalized specific capacity values of the three cells at the 500th, 800th,**
199 **and 1000th cycle. The corresponding electrochemical data for the cells with**

electrolytes containing 0.1 M, 0.5 M, and 1.0 M $LiNO_3$ are recorded in black, red, and blue, respectively.

To better understand the influence of the $LiNO_3$ on the cathode side, scanning electron microscope (SEM) was employed to obtain the morphology of the cycled cathode materials. Figure 2 displayed the SEM images of the (a) GO-S, and (b)-(d) the cathode materials in the cells C-0.1, C-0.5, and C-1.0 cycled for 1000 cycles and stopped at charged states, respectively. The layer-like conjugated structure with highly developed porous flaky structure of the pristine GO-S has been described in our previous studies.[28, 32] The layer-like conjugated structure of the carbon matrix in the cathode materials showed special advantages, including (1) providing the ability to supply good electrical contact between the electrode constituents, (2) accommodating the large volume expansion/shrinkage caused by S-Li_2S conversation during the cell discharge/charge process, and (3) trapping the polysulfides with the porous structure to reduce the shuttle effect.[1, 33-39] These unique properties make the GO a promising candidate as a support and conductive agent in the sulfur electrode. However, GO flakes diminished with cycling and new structures showed up in the cycled materials. Specifically, we found that the sharp porous surface became blurry and the microporous structure of the cathode materials became smoother and less porous. Besides these common structural changes, SEM images also showed some remaining flaky structure of GO, whose amounts are connected to the $LiNO_3$ concentration applied to the cells. In the cathode C-0.1, no or little such layer-like flaky structure was observed; while in the cathodes C-0.5 and C-1.0, obviously more flaky structures were retained; and the cell C-1.0 presented the highest amount of GO persevered. For clear comparison, the GO flakes are pointed out with red arrows in Figures 2 (c) and (d).

The SEM results led to a conclusion that a high concentration of $LiNO_3$ in the electrolyte is essentially beneficial to retain the conjugated structure of the GO in the cathode, which helped to enhance the electrochemical behavior of

the Li-S cells. However, the question why the Li-S cell with electrolyte containing 0.5 M $LiNO_3$ delivered better cell performance compared to the one with higher concentration of $LiNO_3$ still remains. Generally, the morphological change is associated with the changes of the surface chemical properties, which is beyond the information we can get from SEM results. Thus, we employed element-resolved and chemical environment-sensitive spectroscopic technique to gain more details on the cycled sulfur electrodes.

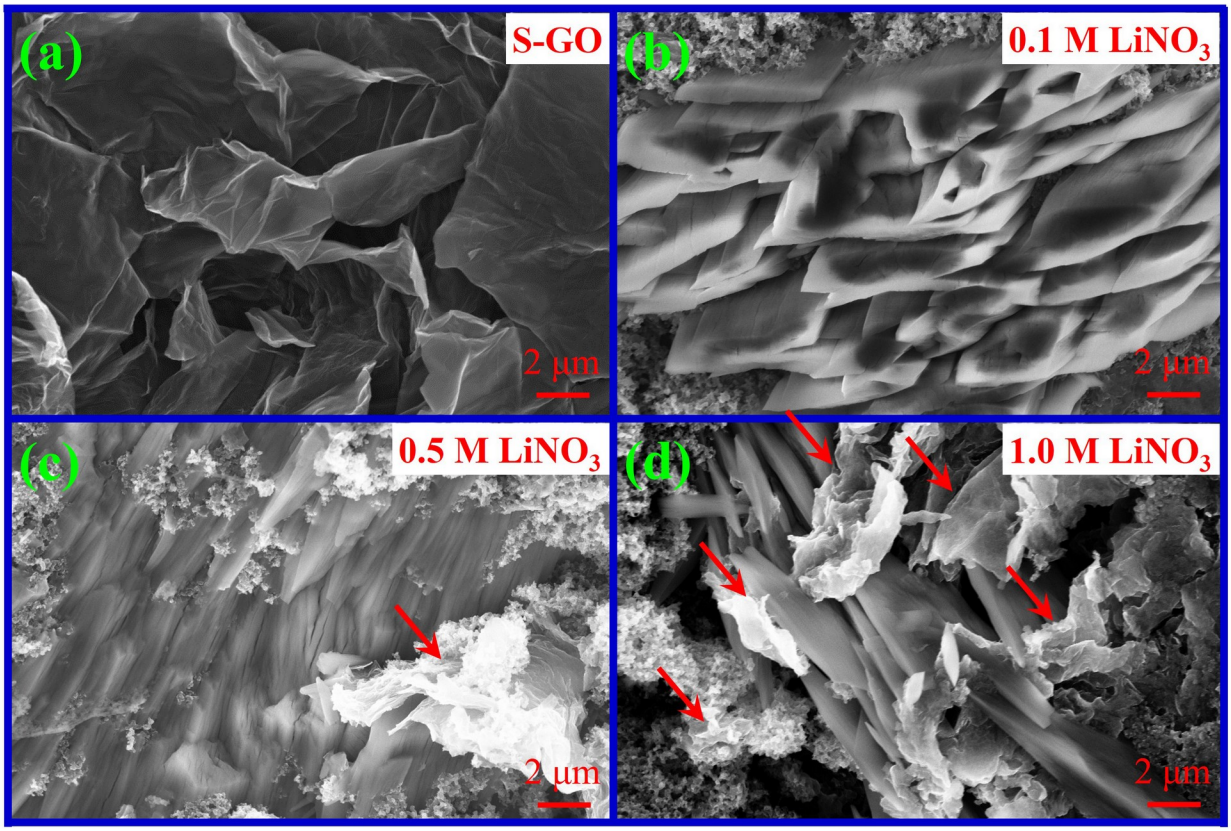

Figure 2: SEM images of the S-GO nano-composites and cathode materials of cycled cells with electrolyte containing (b) 0.1 M, (c) 0.5 M, and (d) 1.0 M $LiNO_3$. The GO flakes have been labeled in the figures with red arrows.

XAS, which probes the transition from the core level to the conduction band, is a powerful technique to investigate the electronic structure and chemical environment of materials. In addition, by recording the absorption signals in

different detection modes, different probing depths can be achieved simultaneously.[40-42] In this work, the TEY and TFY modes, which probe the depths of ~5 nm and ~100 nm layer, respectively, were employed to investigate the sulfur electrodes.[28, 41] The depth profile information provided detailed information on the CEI layer. Taking advantage of the element specificity, different S and C species in the electrodes were separately investigated by measuring the C K-edge and S K-edge signals, respectively.

The SEM images indicated that the GO structure has been damaged during the cell cycling, which is one of the main reasons for the degradation of the cell performances. The C K-edge XAS (Figure 3(a)) tracks the changes of the graphene oxide electronic structure, which will help to reach further understanding of the changes that take place in the sulfur electrode during cycling.

Figure S1 shows the C K-edge XAS spectra of the pristine GO-S sample, which showed spectra similar to those reported previously.[43, 44] After cycling, the C K-edge XAS spectra of the sulfur electrode materials changed, mainly evident as the appearance of a new peak at 290.6 eV, and the decrease of the GO peaks. The intensity of the new peak, assigned to CO_3^{2-}, [27, 32] is associated with the amount of $LiNO_3$ in the cell. Both the surface and bulk signals indicated that the higher concentrations of $LiNO_3$ added to the electrolyte, the smaller amount of CO_3^{2-} formed on the cathode materials. The formation of the CO_3^{2-} layer probably hindered the transportation of the Li ions between the electrolyte and the sulfur during cell operation, which is detrimental to the cell performance.[32] The appearance of the CO_3^{2-} species on the cycled sulfur electrode is an indication of the damage to the GO structure. Hence, the changes of π* peak at 285.5 eV representing the conjugation of the GO structure[44] are detailed.

Figure 3(a) shows that a stronger intensity of the π* peak was observed on both the surface and bulk of the cathode materials as a result of adding higher concentration of $LiNO_3$ to the electrolyte, implying the degradation

degrees of the GO conjugated structure is determined by the $LiNO_3$ concentration. From the peak intensity changes, it is clear that more GO conjugated structure survived during the cell cycling with the presence of $LiNO_3$ of high concentration in the electrolyte, which is consistent with what we obtained from the SEM data. This is understandable due to the catalytic properties of $LiNO_3$ on the transformation from long chain PS to elemental S during the cell charging process.[19] The decreased energy barrier for the reaction reduced the local ion diffusion driven force and hence protected the charge transfer framework, i.e. GO conjugated structure.

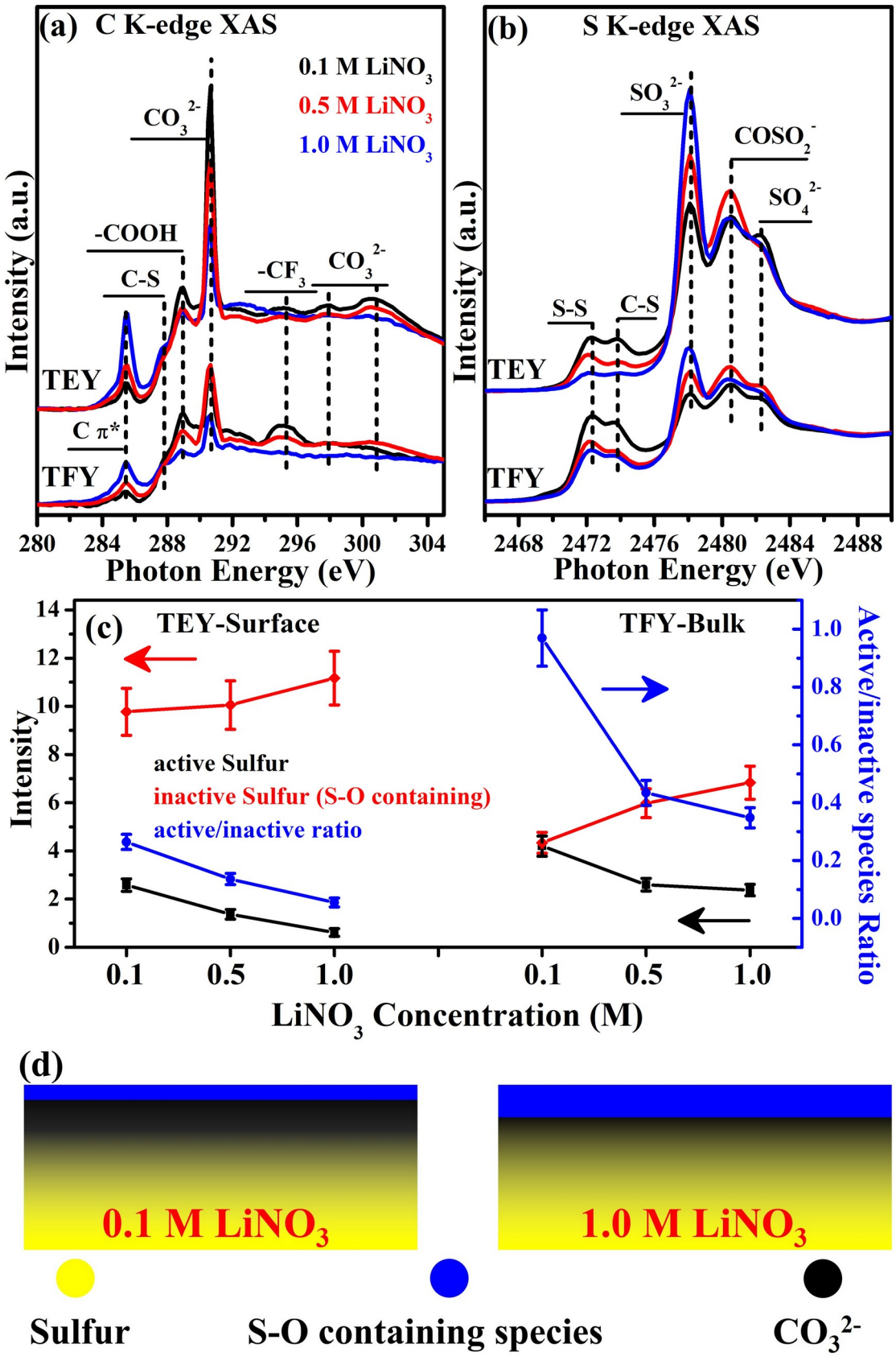
(a) C K-edge XAS
0.1 M LiNO3
0.5 M LiNO3
1.0 M LiNO3
CO3 2-
-COOH
C-S
-CF3
CO3 2-
TEY
C π*
TFY
Intensity (a.u.)
280 284 288 292 296 300 304
Photon Energy (eV)
(b) S K-edge XAS
SO3 2-
COSO2 -
SO4 2-
S-S
C-S
TEY
TFY
Intensity (a.u.)
2468 2472 2476 2480 2484 2488
Photon Energy (eV)
(c) TEY-Surface
TFY-Bulk
active Sulfur
inactive Sulfur (S-O containing)
active/inactive ratio
Intensity
Active/inactive species Ratio
0 2 4 6 8 10 12 14
0.0 0.2 0.4 0.6 0.8 1.0
0.1 0.5 1.0 0.1 0.5 1.0
LiNO3 Concentration (M)
(d)
0.1 M LiNO3
1.0 M LiNO3
Sulfur
S-O containing species
CO3 2-

286

Figure 3: XAS characterization of sulfur electrodes by using (a) C K-edge XAS and (b) S K-edge XAS in both TEY and TFY detection modes. The scale for the TEY spectra was expanded for easy comparison. The sulfur electrodes from the cells C-0.1, C-0.5, and C-1.0 are presented in black, red, and blue lines, respectively. The peaks representing different species are labeled with dashed lines. (c) Intensities of the active S-S and C-S containing species, inactive S-O containing species, and intensity ratio of the active/inactive on the cathode materials of the three cells at both the surface and bulk. The active species, inactive species, the ratio of the active/inactive species were recorded in black, red, and blue, respectively. (d) The schemes representing the distribution of the active sulfur (S-S, C-S), inactive sulfur (SO_3^{2-}, $COSO_2^-$, and SO_4^{2-}), and insulation carbon containing component (CO_3^{2-}) on the cathode materials with 0.1 M and 1.0 M $LiNO_3$ in the electrolyte, respectively. The active sulfur components, insulating S-O containing sulfur components, and insulating CO_3^{2-} layer were displayed in yellow, blue, and black, respectively.

Figure 3(b) shows the S K-edge XAS of the sulfur electrodes in cells cycled with electrolyte containing different concentrations of $LiNO_3$. Five peaks can be observed at 2472.2 eV, 2473.7 eV, 2478.2 eV, 2480.6 eV, and 2482.2 eV, respectively, in the S K-edge XAS spectra. The first two peaks, originating from the S-S and C-S species,[30, 45, 46] represented the recyclable sulfur sources that can participate in the electrochemical reaction. These two peaks are also observed in the spectra of the pristine GO-S sample, shown in Figure S1. After cycling the cell, three peaks, representing SO_3^{2-}, $COSO_2^-$, and SO_4^{2-}, respectively,[27, 28, 47, 48] have appeared up in the high photon energy region, which correspond to species of high valence state. The high valence state species don't participate in the following electrochemical reaction, causing a losses of the cell capacity. These S-O containing compounds are electrical insulators, which are detrimental to the cell performance. It should be noted that the formation of these S-O containing species and the CO_3^{2-} layer as well as the loss of the conjugated structure are observed in Li-S cells with different electrolyte systems, including the classic DOL/DME based electrolyte[27, 32]. The CEI evolution observed in this work

should apply to most Li-S cells. Figure S2 shows the direct comparison of surface- and bulk- sensitive S K-edge spectra of the cathode materials, providing direct observations of the distribution of the S species across the sulfur electrode. It is found that the loss of active recyclable S as well as the accumulation of the inactive S-O containing insulating species were much more obvious on the CEI layer than on the cathode bulk, causing a negative influence on the cell performance.[32] Based on these concepts, the means whereby $LiNO_3$ altered the sulfur electrode, especially the CEI layer, has been quantified by use of the S K-edge XAS spectra.

After subtracting an arctangent background, the spectrum was fitted with several Gaussian peaks, as shown in the Figure S~~2~~3. To get clear comparisons, Figure 3(c) displayed the peak intensity of each compound as a function of the $LiNO_3$ concentrations in the electrolyte. Clearly, the rechargeable S compounds containing S-S and C-S bonds decreased on both the surface and bulk when higher a concentration of $LiNO_3$ was in the electrolyte. On the contrary, the inactive high valence states S species peaks increased with higher concentrations of $LiNO_3$. The promoted side reaction occurring at the CEI layer with high $LiNO_3$ concentration may be connected to the reaction associated with a pronounced additional plateau at the end of the discharge cycle reported previously[49]. In addition, the reported higher over-potential with high $LiNO_3$ concentration can be explained by the formation of more insulating layer at the CEI[49]. Accordingly, it is inferred that high concentrations of $LiNO_3$ in the electrolyte significantly promoted the consumption of the rechargeable S and the formation of insulating species on the CEI layer, which are not beneficial to the cell performance. [50]

Combining the structural changes of C based and S based cathode constituents caused by adding $LiNO_3$ to the electrolyte, how the $LiNO_3$ changed the CEI layer and bulk of the sulfur electrode is schematically presented in Figure 3(d). Essentially, $LiNO_3$ is regarded as a double-edged sword in Li-S cells: (1) on one hand, increasing the $LiNO_3$ concentration

decreased the utilization of S, which is detrimental to the cell performances; and (2) on the other hand, increasing $LiNO_3$ concentrations helped the survival of the GO conjugated structure, which is beneficial to the cell performance. These two competitive effects complicated the understanding of the influence of the $LiNO_3$ on the sulfur electrode. The work reported here helped to rationalize our understanding of the electrochemical behavior of cells with different concentrations of $LiNO_3$. First, the cells C-0.5 and C-1.0 showed the significantly higher coulombic efficiency values, which is due to the strongly promoted retention of the GO conjugated structures due to the higher concentration of $LiNO_3$ in the cell electrolyte. Second, the cell C-0.5 apparently delivered the best capacity stability compared to the other two cells. This is because its sulfur electrode reached a balance state, wherein the conjugated structure of GO was retained while the rechargeable active sulfur was not severely consumed and the inactive sulfur was not significantly accumulated. On the contrary, the other two cells' sulfur electrodes suffered from either the loss of active sulfur species and the accumulation of inactive sulfur species or strongly damaged GO conjugated structure, caused by either high or low concentrations of $LiNO_3$ in the cell electrolyte. To summarize, our study implies that: (1) the coulombic efficiency of the cell during long-term cycling is more related to the structure of the carbon matrix wherein the S is incorporated than the structure of the S species; (2) the real (specific) capacity of the cell is determined by both the structure of the carbon matrix and structure of the S species in the cathode materials.

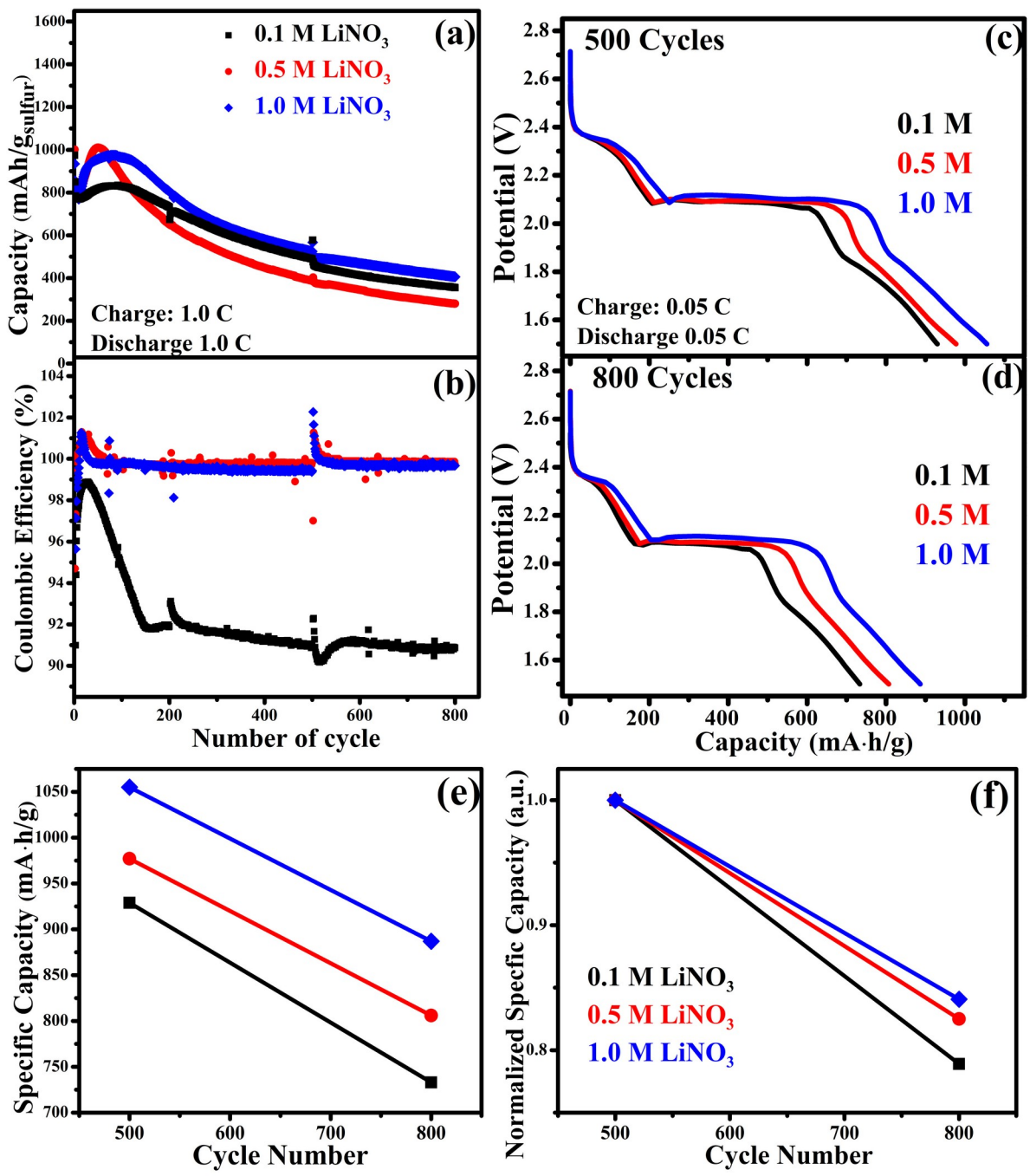

375

376

377 Combining the electrochemical behavior, morphological characterization and
378 the XAS investigations, we propose a detailed mechanism of how $LiNO_3$ in
379 the electrolyte influenced the properties of the CEI layer and sulfur electrode
380 and thus influenced the cell performance. As shown in Figure 4, adding $LiNO_3$

to the electrolyte can simultaneously consume the active sulfur, accumulate the inactive sulfur components and protect the carbon matrix conjugated structure. Thus, an optimal concentration of $LiNO_3$ should be a balance between consuming active sulfur and maintaining the carbon matrix structure.

Finally, we want to point out that the cell activation process is also connected to the $LiNO_3$ concentration in the electrolyte. The normalized capacities (using the initial capacities) of the cells shown in Figure S4 indicated that cells with electrolyte containing 0.5 M $LiNO_3$ showed the earliest activation, while the cells with electrolyte containing 1.0 M $LiNO_3$ demonstrated the longest activation process. In the set of cells C, the cell C-0.5 showed the best activation result, while the cells C-1.0 and C-0.1 showed similar results; in the set of cells CH, the cell CH-1.0 showed the fastest activation, while CH-0.5 and CH-0.1 showed slightly slower activation. All the activation results in the first 100 cycles showed a trend similar to that of the cell performances, which may indicate the activation of the cathode materials may also be controlled by the effects of the consuming of active sulfur and protecting the carbon matrix structure caused by adding $LiNO_3$ to the electrolyte. The detailed mechanism of the activation process of the Li-S cell may need more investigation.

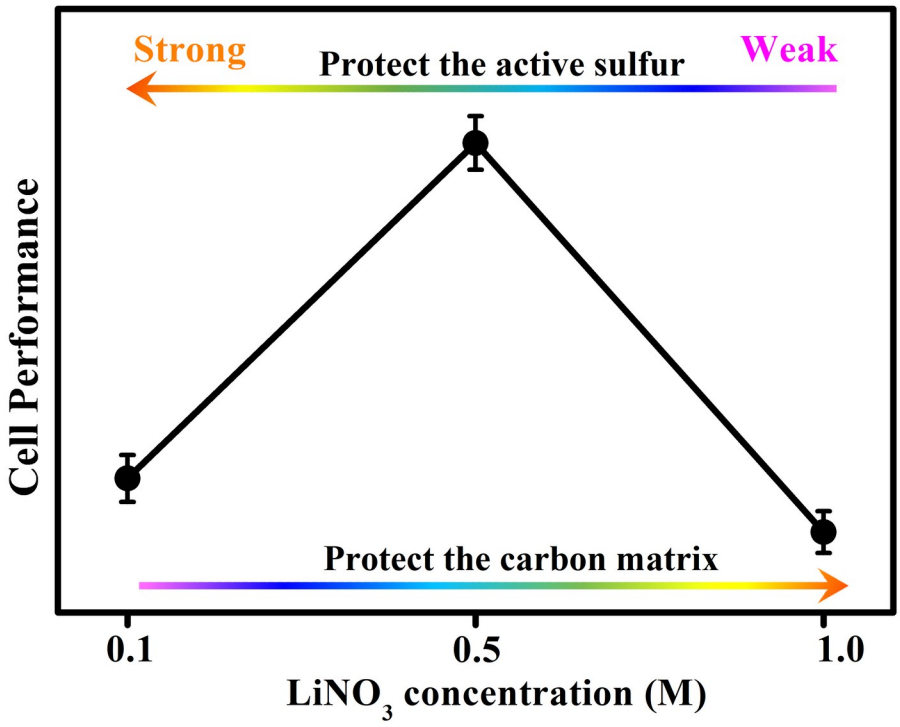

Figure 4: The mechanism of how the $LiNO_3$ in the electrolyte altered the sulfur electrode properties and thus influenced the cell performance.

More broadly, some quintessential information can be obtained to guide the future design of an improved electrolyte for Li-S cells. First, a low $LiNO_3$ concentration is not favorable for cell operation, due to the damage of the carbon matrix structure, which cannot be fully compensated for by the well protected active sulfur. For the use of $LiNO_3$ in Li/S cells, we need to seek an optimum balance concerning the well- retained carbon matrices and the sulfur consumption that produces S-O species. We propose that this balance point is determined by the charge rateas high charge rate requires high charge carrier mobility that is achievable by well- retained carbon matrix conjugated structure. Thus we propose the following possible scenarios: (1) at moderate charge rate, a moderate $LiNO_3$ concentration is desired as the carbon matrix structures are well preserved by using a not too high concentration of $LiNO_3$ and the consumption of the active sulfur should be taken into consideration; (2) at high charge rates, a higher $LiNO_3$

concentration is desired as the carbon matrix structures is preserved, and it is beneficial to the cell performance to protect the carbon matrixes even at the cost of consuming some active sulfur. We believe this strategy may provide some guidance to the advanced cell design and deserve some further investigation.

4. Conclusions:

We have characterized the properties of sulfur electrode materials especially the CEI layer in Li-S cells and the cells' electrochemical behavior to explore the role of $LiNO_3$ in the Li-S cell. We found that $LiNO_3$ can increase the consumption of the active sulfur and help to protect the carbon matrix structure. These competitive effects on the cell performance determined that a proper concentration of $LiNO_3$ is required to achieve the most optimized cell performance. Our study reported new and direct evidence of how the $LiNO_3$ in the electrolyte changes the properties of the sulfur electrode and thus influences the cell performance. The results provide new insight on the effect of $LiNO_3$ on the Li-S cell, establishing a possibility of providing a new strategy to explore and develop better $LiNO_3$-containing electrolytes for advanced Li-S cells that can be used for scaled-up applications. This work also illustrated the capability of synchrotron X-ray techniques to provide unique information regarding the electronic structure and its potential to help understand the properties of the materials.

References:

[1] M.-K. Song, Y. Zhang, E.J. Cairns, Nano Letters, 13 (2013) 5891-5899.
[2] M.-K. Song, E.J. Cairns, Y. Zhang, Nanoscale, 5 (2013) 2186-2204.
[3] P.G. Bruce, S.A. Freunberger, L.J. Hardwick, J.-M. Tarascon, Nat Mater, 11 (2012) 19-29.
[4] X. Ji, L.F. Nazar, Journal of Materials Chemistry, 20 (2010) 9821-9826.
[5] A. Manthiram, Y. Fu, S.-H. Chung, C. Zu, Y.-S. Su, Chemical Reviews, 114 (2014) 11751-11787.
[6] Y.V. Mikhaylik, J.R. Akridge, Journal of The Electrochemical Society, 151 (2004) A1969-A1976.

[7] Y. Yang, G. Zheng, Y. Cui, Chemical Society Reviews, 42 (2013) 3018-3032.
[8] G. Ai, Y. Dai, Y. Ye, W. Mao, Z. Wang, H. Zhao, Y. Chen, J. Zhu, Y. Fu, V. Battaglia, J. Guo, V. Srinivasan, G. Liu, Nano Energy, 16 (2015) 28-37.
[9] M.J. Lacey, A. Yalamanchili, J. Maibach, C. Tengstedt, K. Edstrom, D. Brandell, RSC Advances, 6 (2016) 3632-3641.
[10] Y.V. Mikhaylik, Google Patents2008.
[11] N. Ding, L. Zhou, C. Zhou, D. Geng, J. Yang, S.W. Chien, Z. Liu, M.-F. Ng, A. Yu, T.S.A. Hor, M.B. Sullivan, Y. Zong, Scientific Reports, 6 (2016) 33154-33163.
[12] W. Li, H. Yao, K. Yan, G. Zheng, Z. Liang, Y.-M. Chiang, Y. Cui, Nature Communications, 6 (2015) 7436-7444.
[13] S. Xiong, K. Xie, Y. Diao, X. Hong, Electrochimica Acta, 83 (2012) 78-86.
[14] L. Zhang, M. Ling, J. Feng, L. Mai, G. Liu, J. Guo, Energy Storage Materials, 11 (2018) 24-29.
[15] S.S. Zhang, Journal of Power Sources, 162 (2006) 1379-1394.
[16] S.S. Zhang, Electrochimica Acta, 70 (2012) 344-348.
[17] S.S. Zhang, Electrochimica Acta, 97 (2013) 226-230.
[18] S.S. Zhang, Journal of The Electrochemical Society, 159 (2012) A920-A923.
[19] S.S. Zhang, Journal of Power Sources, 322 (2016) 99-105.
[20] B.D. Adams, E.V. Carino, J.G. Connell, K.S. Han, R. Cao, J. Chen, J. Zheng, Q. Li, K.T. Mueller, W.A. Henderson, J.-G. Zhang, Nano Energy, 40 (2017) 607-617.
[21] A. Jozwiuk, B.B. Berkes, T. Weiß, H. Sommer, J. Janek, T. Brezesinski, Energy & Environmental Science, 9 (2016) 2603-2608.
[22] R. Xu, J.C.M. Li, J. Lu, K. Amine, I. Belharouak, Journal of Materials Chemistry A, 3 (2015) 4170-4179.
[23] F.C.d. Godoi, D.-W. Wang, Q. Zeng, K.-H. Wu, I.R. Gentle, Journal of Power Sources, 288 (2015) 13-19.
[24] M. Ebadi, M.J. Lacey, D. Brandell, C.M. Araujo, The Journal of Physical Chemistry C, 121 (2017) 23324-23332.
[25] X. Yu, A. Manthiram, Accounts of Chemical Research, 50 (2017) 2653-2660.
[26] T. Tao, S. Lu, Y. Fan, W. Lei, S. Huang, Y. Chen, Advanced Materials, 29 (2017) 1700542-1700560.
[27] Y. Ye, A. Kawase, M.-K. Song, B. Feng, Y.-S. Liu, M. Marcus, J. Feng, E. Cairns, J. Guo, J. Zhu, Nanomaterials, 6 (2016) 14-23.

[28] Y. Ye, A. Kawase, M.-K. Song, B. Feng, Y.-S. Liu, M.A. Marcus, J. Feng, H. Fang, E.J. Cairns, J. Zhu, J. Guo, The Journal of Physical Chemistry C, 120 (2016) 10111-10117.
[29] K.H. Wujcik, T.A. Pascal, C.D. Pemmaraju, D. Devaux, W.C. Stolte, N.P. Balsara, D. Prendergast, Advanced Energy Materials, 5 (2015) 1500285-1500294.
[30] T.A. Pascal, K.H. Wujcik, J. Velasco-Velez, C. Wu, A.A. Teran, M. Kapilashrami, J. Cabana, J. Guo, M. Salmeron, N. Balsara, D. Prendergast, The Journal of Physical Chemistry Letters, 5 (2014) 1547-1551.
[31] M. Ling, L. Zhang, T. Zheng, J. Feng, J. Guo, L. Mai, G. Liu, Nano Energy, 38 (2017) 82-90.
[32] X. Feng, M.-K. Song, W.C. Stolte, D. Gardenghi, D. Zhang, X. Sun, J. Zhu, E.J. Cairns, J. Guo, Physical Chemistry Chemical Physics, 16 (2014) 16931-16940.
[33] L. Ji, M. Rao, H. Zheng, L. Zhang, Y. Li, W. Duan, J. Guo, E.J. Cairns, Y. Zhang, Journal of the American Chemical Society, 133 (2011) 18522-18525.
[34] Y. Qiu, W. Li, W. Zhao, G. Li, Y. Hou, M. Liu, L. Zhou, F. Ye, H. Li, Z. Wei, S. Yang, W. Duan, Y. Ye, J. Guo, Y. Zhang, Nano Letters, 14 (2014) 4821-4827.
[35] J. Xie, H.-J. Peng, J.-Q. Huang, W.-T. Xu, X. Chen, Q. Zhang, Angewandte Chemie, 56 (2017) 16223-16227.
[36] Y. Hwa, H.K. Seo, J.-m. Yuk, E.J. Cairns, Nano Letters, 17 (2017) 7086-7094.
[37] Y. Chen, S. Choi, D. Su, X. Gao, G. Wang, Nano Energy, Just Accepted (2018).
[38] S. Wu, R. Ge, M. Lu, R. Xu, Z. Zhang, Nano Energy, 15 (2015) 379-405.
[39] F. Li, X. Jiang, J. Zhao, S. Zhang, Nano Energy, 16 (2015) 488-515.
[40] Y. Ye, M. Kapilashrami, C.-H. Chuang, Y.-s. Liu, P.-A. Glans, J. Guo, MRS Communications, 7 (2017) 53-66.
[41] Y. Ye, J.E. Thorne, C.H. Wu, Y.-S. Liu, C. Du, J.-W. Jang, E. Liu, D. Wang, J. Guo, The Journal of Physical Chemistry B, 122 (2018) 927-932.
[42] Y. Ye, C.H. Wu, L. Zhang, Y.-S. Liu, P.-A. Glans-Suzuki, J. Guo, Journal of Electron Spectroscopy and Related Phenomena, 221 (2017) 2-9.
[43] C.-H. Chuang, S.C. Ray, D. Mazumder, S. Sharma, A. Ganguly, P. Papakonstantinou, J.-W. Chiou, H.-M. Tsai, H.-W. Shiu, C.-H. Chen, H.-J. Lin, J. Guo, W.-F. Pong, Scientific Reports, 7 (2017) 42235-42244.
[44] C.H. Chuang, Y.F. Wang, Y.C. Shao, Y.C. Yeh, D.Y. Wang, C.W. Chen, J.W. Chiou, S.C. Ray, W.F. Pong, L. Zhang, J.F. Zhu, J.H. Guo, Scientific Reports, 4 (2014) 4525-4531.

[45] M. Cuisinier, P.-E. Cabelguen, S. Evers, G. He, M. Kolbeck, A. Garsuch, T. Bolin, M. Balasubramanian, L.F. Nazar, The Journal of Physical Chemistry Letters, 4 (2013) 3227-3232.
[46] N. Kornienko, J. Resasco, N. Becknell, C.-M. Jiang, Y.-S. Liu, K. Nie, X. Sun, J. Guo, S.R. Leone, P. Yang, Journal of the American Chemical Society, 137 (2015) 7448-7455.
[47] A. Vairavamurthy, Spectrochimica Acta Part A: Molecular and Biomolecular Spectroscopy, 54 (1998) 2009-2017.
[48] F. Jalilehvand, Chemical Society Reviews, 35 (2006) 1256-1268.
[49] A. Jozwiuk, H. Sommer, J. Janek, T. Brezesinski, Journal of Power Sources, 296 (2015) 454-461.
[50] X.-B. Cheng, C. Yan, X. Chen, C. Guan, J.-Q. Huang, H.-J. Peng, R. Zhang, S.-T. Yang, Q. Zhang, Chem, 2 (2017) 258-270.